

Strong-Weak Integrated Semi-supervision for Unsupervised Single and Multi Target Domain Adaptation

Xiaohu Lu and Hayder Radha, *Fellow, IEEE*

Abstract—Unsupervised domain adaptation (UDA) focuses on transferring knowledge learned in the labeled source domain to the unlabeled target domain. Despite significant progress that has been achieved in single-target domain adaptation for image classification in recent years, the extension from single-target to multi-target domain adaptation is still a largely unexplored problem area. In general, unsupervised domain adaptation faces a major challenge when attempting to learn reliable information from a single unlabeled target domain. Increasing the number of unlabeled target domains further exacerbate the problem rather significantly. In this paper, we propose a novel *strong-weak integrated semi-supervision (SWISS)* learning strategy for image classification using unsupervised domain adaptation that works well for both single-target and multi-target scenarios. Under the proposed SWISS-UDA framework, a strong representative set with high confidence but low diversity target domain samples and a weak representative set with low confidence but high diversity target domain samples are updated constantly during the training process. Both sets are fused randomly to generate an augmented strong-weak training batch with pseudo-labels to train the network during every iteration. The extension from single-target to multi-target domain adaptation is accomplished by exploring the class-wise distance relationship between domains and replacing the strong representative set with much stronger samples from peer domains via *peer scaffolding*. Moreover, a novel adversarial logit loss is proposed to reduce the intra-class divergence between source and target domains, which is back-propagated adversarially with a gradient reverse layer between the classifier and the rest of the network. Experimental results based on three popular benchmarks, Office-31, Office-Home, and DomainNet, show the effectiveness of the proposed SWISS framework with our method achieving the best performance in both Office-Home and DomainNet with improvement margins of 0.4% and 1.0%, respectively.

Index Terms—Domain adaptation, unsupervised, multi-target, peer scaffolding, intra-class divergence.

I. INTRODUCTION

THE success of deep neural networks in tackling critical tasks, such as image classification [1], object detection [2], [3], semantic segmentation [4], and image captioning is highly dependent on the availability of large amount of labeled training samples. Meanwhile, the generalization ability of deep neural networks is poor when applied to different target domains. The inclusion of additional labeled samples for the target domains can be a straightforward solution to this deficiency; but such a solution is arguably inefficient and costly.

Unsupervised domain adaptation (UDA) tackles this problem by transferring the knowledge learned in the labeled

source domain to the unlabeled target domain. This transferance is usually accomplished by aligning the distributions of data points in source domain and target domain such that the classifier trained on the source domain can also be applied onto the target domain. Most current domain alignment methods can be classified into two categories: moment matching based and adversarial learning based. The idea of moment matching is based on the observation that two distributions are similar if their moments in different orders are all close to each other [5]. The Maximum Mean Discrepancy (MMD) [6] approach is widely used by this type of methods, which attempt to align domains through minimizing the distance between weighted sums of all raw moments. Another popular paradigm is leveraging the idea of adversarial learning [7] that is rooted in Generative Adversarial Networks (GANs) [8]. This approach is based on (a) training a domain classifier to align domains' distributions; yet (b) trying to trick or confuse the domain classifier in differentiating between source and target domain data by generating domain-invariant features. Hence, the adversarial learning is usually performed between the feature generator and the domain classifier so that when the domain classifier is fully confused by the feature generator the goal of domains' alignment is achieved. Despite the fact that most of recent works on domain adaptation still focus mainly on the the single-target scenario, it is noteworthy that multi-target domain adaptation has been drawing increasing attention.

Multi-target UDA [9]–[14] assumes that there exists only one source domain, but the target domain samples are collected from several different distributions. The goal of multi-target UDA is to transfer the knowledge learned from the source domain to diverse target domains. Another objective is to explore the underlying relationships and patterns among target domains, such that the performance of each target domain in multi-target UDA is better than that of training several single-source single-target UDA networks separately. Currently, there exist only few works on multi-target UDA, including the attention guided method [9], [10], mutual information based method [11], knowledge distillation based method [12], and collaborative consistency learning [13].

Despite the fact that significant progress in single-target UDA and some noteworthy advancement in multi-target domain adaptation areas have been achieved individually, a unified framework that can work for both areas is still missing. In this paper, we address this problem by proposing a strong-weak integrated semi-supervision (SWISS) learning strategy

that maintains a strong representative set with high confidence but low diversity samples and a weak representative set with low confidence but high diversity samples in the full training process. Furthermore, the proposed SWISS framework generates augmented training samples with pseudo-labels from these two representative sets to train the network in each iteration. Both single-target and multi-target UDA can be handled in a viable manner under the proposed framework. The extension from single-target to multi-target UDA is achieved by adopting the *peer scaffolding* strategy [15], which updates the strong representative set with samples not only from the target domain itself but also from its peer domains. Moreover, we also propose a novel adversarial logit loss to improve the performance by reducing the intra-class divergence between source and target domains. In summary, our contributions in this paper¹:

- Developing a unified framework for both single and multiple target domain adaptation via strong-weak integrated semi-supervision.
- Adopting the peer scaffolding theory [15], which has been developed and studied in the general field of education, to learn from peer domains in the multi-target UDA scenario.
- Introducing a novel adversarial logit loss function that can reduce the intra-class domain divergence.
- Demonstrating that the proposed SWISS framework achieves state-of-the-art performance in several public benchmarks.

II. RELATED WORK

A. Unsupervised Domain Adaptation

Most early unsupervised domain adaptation methods in the area of image classification utilized moment matching strategy to align data distributions in the source and target domains. For example, in the work of [17], they used one kernel function and one adaptation layer for moment matching. Long et al. [18] extended this strategy to include multiple kernels and adaptation layers, which led to better performance. Later on, Ganin et al. [19] introduced the idea of adversarial learning to domain adaptation by training a binary domain classifier to distinguish the data points from different domains. Based on this idea, most of the later methods explored additional information to further help domains' alignment. For example, in the work of [20], the prediction scores were combined with the feature vector of the data as conditional information to align the domains. In the work of [21], the gradient discrepancy between source samples and target samples is minimized to improve the accuracy by introducing semantic information of target samples. Similarly, in another work of [22], an auxiliary classifier only for target data is designed to improve the quality of pseudo labels, which is then utilized for training the network via cross-entropy loss. Meanwhile, in the work of [23], training

samples from augmented-domains between the source domain and target domain are generated by a fixed ratio-based mixup strategy, which are applied along with two confidence based learning methodologies to train the model. While some of these methods have demonstrated promising results on public benchmarks, directly applying them to multi-target domain adaptation may not lead to performance improvements [13]. Therefore, it is essential to develop dedicated approaches that specifically address the challenges posed by multi-target domain adaptation.

B. Multi-target Domain Adaptation

The topic of multi-target unsupervised domain adaptation (UDA) has received relatively less attention, with only a few works [9]–[14] addressing this specific problem. Most of these works primarily focus on the association between target domains. For example, in the work of [9], a unified subspace common for all domains with a heterogeneous graph attention network is learned to propagate semantic information among domains. Similarly, in the work of [10] an attention guided method is proposed to capture the context dependency information on transferable regions among the source and target domains. While in [12], a multi-teacher knowledge distillation method is proposed to iteratively distill the target domain knowledge to a common space. Moreover, in the work of [11], a unified mutual information based approach is developed to learn both shared and private information in different domains. Recently, in the work of [14], the graph convolutional network is adopted to aggregate features across domains, which is cooperating with a curriculum learning strategy to improve the final performance in multi-target domain adaptation. Despite the progress made in this field, there still exists a significant performance gap between these multi-target domain adaptation methods and the state-of-the-art single-target domain adaptation methods. Further research and innovation are needed to bridge this gap and develop more effective approaches for multi-target UDA.

C. Semi-supervised Learning

Similar to unsupervised domain adaptation, semi-supervised learning [24]–[26] also focuses on tackling labeled and unlabeled samples. In order to make use of unlabeled data, semi-supervised learning methods assume that there exist some underlying relationships between distributions of data. Based on this assumption, several categories of methods are developed. Pseudo-label based methods [24] select high-confidence predictions as the label for unlabeled samples. Information maximization based methods [27] consider that a good distribution should be individually certain and globally diverse, and utilize the information maximization loss to regularize the unlabeled samples. Regularization and normalization based methods [25], [26] adopt regularization and normalization strategies, e.g., batch normalization, to reduce the model's bias to the source domain such that the model's performance in target domain can be improved. Recently, an increasing number of researchers in unsupervised domain adaptation seek to borrow ideas from semi-supervised learning. For example,

¹This paper represents a significantly expanded version of our recent conference paper [16]. This includes generalizing our SWISS framework to address the problem of multi-target unsupervised domain adaptation. Another new contribution of this paper is the novel UDA approach that is based on scaffolding theory.

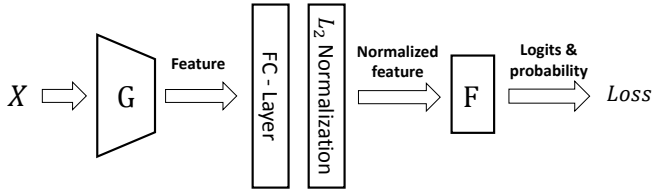


Fig. 1. The high-level architecture of the baseline network used in our unsupervised domain adaptation method. For forwarding, training samples are fed into a generator \mathbf{G} , followed by a bottleneck network formed by a Fully Connected (FC) layer and a L_2 normalization layer, and a classifier \mathbf{F} .

[28] assigned pseudo-labels with highest confidence to unlabeled samples, while in the work of [29] the information maximization loss is adopted to improve performance of domain adaptation.

D. Peer Scaffolding

The concept of peer scaffolding finds its roots in the field of education, where it has been widely employed to enhance students' learning experiences through support from others. This approach is based on the idea that learners can benefit from interactions with more knowledgeable individuals, such as teachers or peers who excel in a particular domain. Peer scaffolding has been extensively studied and evaluated in educational settings, particularly in collaborative activities within classrooms. Previous research has demonstrated the effectiveness of peer scaffolding in various educational contexts. For example, in the domain of writing, Riazi et al. [30] found that peer scaffolding activities significantly improved students' writing quality during the revision process. Additionally, the work of [31] suggests that incorporating peer scaffolding systems into pedagogical approaches can enhance students' learning processes. Overall, the underlying principle of peer scaffolding is to leverage the knowledge and support of others to facilitate individual learning and achieve better learning outcomes.

III. METHODOLOGY

A. Network Architecture

Fig. 1 shows the high-level architecture of our *baseline network* that includes a feature generator network \mathbf{G} , a bottleneck network formed by a Fully Connected (FC) layer and a L_2 normalization layer, and a classifier network \mathbf{F} . For \mathbf{G} , we employ the pre-trained ResNet-50 or ResNet-101 [1] as the backbone. For the bottleneck network, the output dimension of the FC-layer is 1024, the L_2 normalization layer normalizes and scales the feature vector of each input training sample into a normalized feature vector with the L_2 norm being a constant value T . The classifier network \mathbf{F} is formed by k sub-classifiers corresponding to the k classes. In the forwarding path, for an image x from the input batch X , regardless of its domain, we firstly feed it into \mathbf{G} to generate a 1024-d feature vector $\mathbf{G}(x)$. Then, we calculate the logits $\{l_1, l_2, \dots, l_k\}$ between the normalized feature and each sub-classifier using the inner product, and estimate the prediction probabilities of the normalized feature belonging to

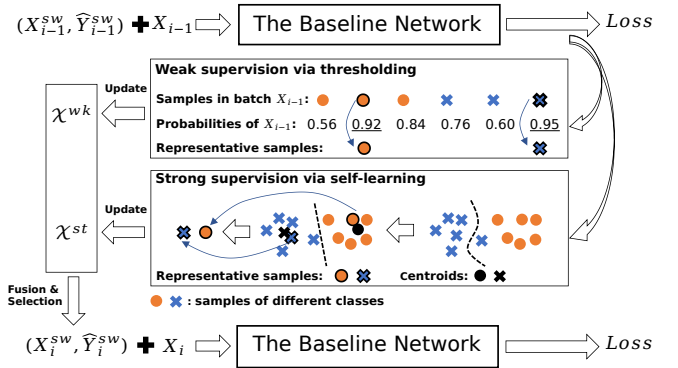


Fig. 2. The pipeline of our strong-weak integrated semi-supervision method for typical single-source single-target domain adaptation. A weak representative set \mathcal{X}^{wk} and a strong representative set \mathcal{X}^{st} are maintained during the training process. A strong-weak integrated semi-supervision set of training samples $(X_i^{sw}, \hat{Y}_i^{sw})$ is generated to train the baseline network.

each class as $\{p_1, p_2, \dots, p_k\} = \sigma(\{l_1, l_2, \dots, l_k\})$ with σ being the softmax function. After that, we calculate the loss terms based on the logits and probabilities.

B. Strong-weak Integrated Semi-supervision for Single-target UDA

Fig. 2 shows the pipeline of our strong-weak integrated semi-supervision method for the typical single-source single-target domain adaptation. The key idea is to obtain a strong representative set \mathcal{X}^{st} and a relatively weak representative set \mathcal{X}^{wk} and then fuse them to generate reliable and diverse augmented samples to train the network. The weak representative set \mathcal{X}^{wk} is updated by target samples with prediction probability higher than a threshold after every iteration. While the strong representative set \mathcal{X}^{st} is formed by target samples with the highest confidence of belonging to each class, which is updated every pre-specified number of iterations via self-learning. In the i_{th} iteration of training, the samples of each class in \mathcal{X}^{wk} and \mathcal{X}^{st} are fused to form an augmented supervision set with pseudo-labels $(X_i^{sw}, \hat{Y}_i^{sw})$, which along with the target-domain batch X_i are utilized to train the baseline network. The rationale for this strong-weak integrated semi-supervision is that the strong representative set \mathcal{X}^{st} is of highest prediction confidence but lower diversity, while the weak representative set \mathcal{X}^{wk} is less reliable in prediction but with much higher in diversity. Hence, the combination of both sets gives a good balance between prediction confidence and diversity for the augmented training samples.

1) *Strong Supervision via Self-learning*: We adopt the same self-learning strategy as in [21] to get the strong representative set \mathcal{X}^{st} . Namely, given the target domain sample set $\{x_i\}_{i=1}^n$ with n samples and the baseline network as shown in Fig. 1, there are three steps. Firstly, the prediction probabilities and the normalized feature vectors of training samples in the target domain are obtained by feeding the target domain samples into the baseline network. The concatenation of these probabilities P is a $n \times k$ matrix, and that of the normalized feature vectors V is a $n \times d$ matrix. Here n is the number of target domain samples, k is the number of classes, $d = 1024$ is the dimension of feature vector.

Then, the initial centroid of class j is obtained as:

$$c_j^{(0)} = \frac{P_{:,j}^T V}{\sum_j P_{:,j}}, \quad (1)$$

where $P_{:,j}$ denotes the j th column of the probability matrix, which corresponds to class j . After that, the initial self-supervised pseudo-label can be obtained by assigning each sample to the class with closest centroid as:

$$\hat{y}^{(0)} = \arg \min_j D(v, c_j^{(0)}) \quad (2)$$

where v represents the normalized feature vector of a target domain sample, and $D(\cdot)$ measures the cosine distance between two vectors.

Finally, the class centroids are recalculated by replacing the probability matrix P with a $n \times k$ one-hot distribution matrix $\mathbb{1}$ obtained from the initial self-supervised pseudo-label $\hat{y}^{(0)}$, and the strong representative set \mathcal{X}^{st} is obtained by selecting the target samples closest to each class centroids. Namely, for a specific class j ,

$$\begin{aligned} c_j^{(1)} &= \frac{\mathbb{1}_{:,j}^T V}{\sum_j \mathbb{1}_{:,j}}, \\ x_j^{st} &= x_{\arg \min_{i \in [1, n]} D(v_i, c_j^{(1)})} \end{aligned} \quad (3)$$

where $\mathcal{X}^{st} = \{x_j^{st}\}_{j \in [1, k]}$, n is the number of target samples, k is the number of classes.

Under this self-learning strategy, the distribution of the pseudo-labels will be slightly shifted toward the target domain by assigning each target sample to the closest class' center in a self-supervised way. This self-learning procedure is performed every pre-specified number of iterations, e.g., 200 iterations, and only the samples with closest distances to the centroids of each class are selected as shown in Fig.2. Note that those strong samples usually have high prediction confidence, which means that they are generally closer to the source domain than other target domain samples. Beside, they are also robust against noise because of the robustness of centroids. For example, some outlier target domain samples may have high prediction probabilities by accident, but they will not be selected as strong representative samples in our method because they are far away from the centroids in the feature space. Based on these two properties, we consider this set of target domain samples as the "strong" one in comparison with the weak supervision set that is introduced below.

2) *Weak Supervision via Thresholding*: For weak supervision, we employ a higher updating frequency than the strong supervision. And, we adopt a simple thresholding strategy to update \mathcal{X}^{wk} for each batch of target samples. More specifically, after inputting a target batch $X = \{x_i\}_{i=1}^{b_s}$ with size b_s to the baseline network, we identify the highest probabilities $\mathbf{p} = \{p_i\}_{i=1}^{b_s}$ and the corresponding pseudo-labels $\mathbf{l} = \{l_i\}_{i=1}^{b_s}$ for the b_s samples in the batch. Then, for each class j that has an entry in the pseudo-label vector \mathbf{l} , the sample with the highest probability (which must be greater than a threshold λ) of belonging to this class j is selected as the new representative sample for that class j . In other words, under the weak supervision learning process, there is a single and unique

representative sample x_j^{wk} for any class j at any given time. Hence, a new sample could potentially be used to update the corresponding representative sample x_j^{wk} for class j in the current weak set \mathcal{X}^{wk} . Namely,

$$\begin{aligned} x_j^{wk} &= x_{\arg \max_i p_i}, \\ \text{s.t. } l_i &= j, p_i > \lambda, \end{aligned} \quad (4)$$

where $\mathcal{X}^{wk} = \{x_j^{wk}\}_{j \in [1, k]}$, k is the number of classes.

3) *Strong-weak Fusion*: In practice, we find that simply using the strong supervision can only slightly reduce the domain divergence. This is because the network can easily over-fit on the strong representative set by remembering them instead of learning knowledge from them due to the small amount of samples in \mathcal{X}^{st} (one sample per class). Meanwhile, in the case of weak supervision only, the discriminability of the network maybe impaired under challenging scenarios due to the error associated with predicting the pseudo-labels in \mathcal{X}^{wk} . Fusing both \mathcal{X}^{st} and \mathcal{X}^{wk} can achieve a good balance between them, and consequently, such fusion achieves smaller domain divergence and higher discriminability. Therefore, we adopt a random fusion strategy to generate the fused strong-weak representative set \mathcal{X}^{sw} :

$$x_j^{sw} = r x_j^{st} + (1 - r) x_j^{wk}, \text{ s.t. } r \in (0, 1), \quad (5)$$

where x_j^{st} and x_j^{wk} are the representative images for class j , x_j^{sw} is the fused one in the pixel domain, r is a random number in $(0, 1)$. The reason for using a random value instead of a constant one for r is to increase the diversity of the strong-weak representative set \mathcal{X}^{sw} . In practice, we find that adding the full set of \mathcal{X}^{sw} along with the corresponding pseudo-label as supervision may override the target domain itself when the number of classes k is much greater than the batch size, e.g., $k=345$ in DomainNet. Therefore, we only select a small batch X^{sw} from \mathcal{X}^{sw} according to the data distribution of the input batch. Namely, given the input batch X and its most-likely class label \hat{Y} which is obtained from the estimated probability, we have

$$X^{sw} = \{x_i^{sw}\}_{i \in \hat{Y}}. \quad (6)$$

Finally, the selected batch of images along with the corresponding label (X^{sw}, \hat{Y}^{sw}) are utilized to train the baseline network.

4) *Pipeline for Single-target UDA*: The pipeline for our strong-weak supervision for single-target domain adaptation can be found in Alg. 1. Note that at the beginning of training, both \mathcal{X}^{st} and \mathcal{X}^{wk} are empty, which are only utilized for training after being initialized in the first updating of the strong representative set. Details about the loss functions used in Alg. 1 will be introduced in Sec. III-D.

C. Strong-weak Integrated Semi-supervision for Multi-target UDA

To extend a typical domain adaptation method from single-target to multi-target, a straightforward approach would be to combine all the target domains into a single one. However, it has been noted in prior work [9] that simply combining samples from all target domains can actually degrade performance, as the divergence between certain target domains can

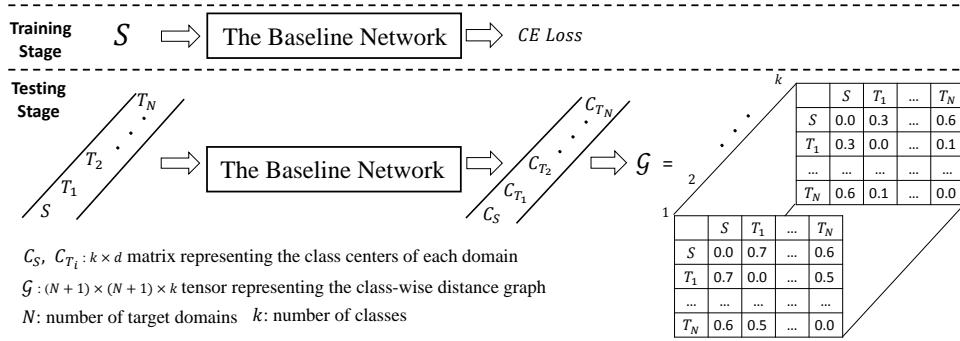


Fig. 3. A demonstration on how we apply a two-stage strategy to get the class-wise distance graph for peer scaffolding. A baseline network on the labeled source domain in the training stage. Then each domain is fed into the trained baseline network to calculate the class centers. Finally, a class-wise distance graph is generated to represent the distance between different domains.

Algorithm 1 Strong-Weak Integrated Semi-Supervision (SWISS) for single-target domain adaptation

Require: a labeled source domain S , an unlabeled target domain T

Ensure: optimized parameters of a baseline network as Fig. 1

initialize generator \mathcal{G} with pre-trained ResNet

for each iteration **do**

$L_{CE} \leftarrow$ forward a source batch (X^s, Y^s) to network

Back-propagate L_{CE} , optimization

$L_{IM}, L_{ALL} \leftarrow$ forward a batch X^t to network

$(X^{sw}, \hat{Y}^{sw}) \leftarrow$ sample fusion and selection

$L_{SW} \leftarrow$ forward (X^{sw}, \hat{Y}^{sw}) to network

Back-propagate $k1L_{IM} + k2L_{ALL} + k3L_{SW}$

$\mathcal{X}^{wk} \leftarrow$ weak representative set updating

if reach certain iterations **then**

$\mathcal{X}^{st} \leftarrow$ strong representative set updating

end if

end for

be larger than the divergence between the source domain and each target domain individually. To address this challenge, we draw inspiration from the concept of “peer scaffolding” in the education field [30]. This involves allowing each target domain to learn not only from the source domain but also from peer domains that share similarities with the target domain. By identifying these peer domains, we can update the strong representative set \mathcal{X}^{st} accordingly, incorporating stronger samples from relevant peer domains. Furthermore, for the weak representative set \mathcal{X}^{wk} , we employ the same thresholding strategy as described in Sec. III-B.

1) *Class-wise Peer Scaffolding*: In the context of peer scaffolding [30], a crucial aspect is determining the “more knowledgeable peers” from whom to learn. In the domain adaptation scenario, the notion of “more knowledgeable” typically refers to domains that exhibit smaller divergence from the source domain. Some popular domain divergence measures include the KL-divergence [32], covariance [33], \mathcal{H} -divergence [34], and Maximum Mean Discrepancy [35]. However, most of them are designed to estimate the overall domain divergence, which may not be accurate when the domain divergence shows some class-relevant properties. In this work, we find that the cosine distance between centroids of different classes can be a good measure for *class-wise peer scaffolding*. More specifically, given a labeled source domain S , and N unlabeled target domains $\{T_i\}_{i=1}^N$, we use the

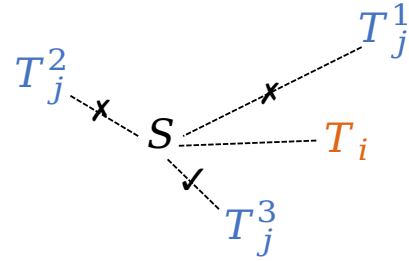


Fig. 4. A demonstration on the two criteria for peer scaffolding. Location 3 of T_j^3 satisfies both criteria, therefore it can be used to reduce the domain divergence between S and T_i .

following two-stage strategy to obtain a $(N+1) \times (N+1) \times k$ tensor \mathcal{G} to represent the class-wise distance graph between each pair of domains:

- For the training stage, we train a baseline network on the labeled source domain with the widely used Cross Entropy loss. To avoid over-fitting on the source domain, we stop the training if the prediction accuracy on the source domain starts to decrease.
- For the testing stage, we feed each domain’s samples into the trained network to get a $n \times k$ probabilities matrix P and a $n \times d$ feature matrix V . Here n and k denote the number of samples and classes in the domain, respectively. Then the centroid of each class is obtained in the same way as introduced in Eq. 1. The combination of those k centroids forms a $k \times d$ centroid matrix C . Then, given the centroid matrices of source domain C_S and all the target domains $\{C_{T_i}\}_{i=1}^N$, a $(N+1) \times (N+1) \times k$ tensor \mathcal{G} can be obtained by calculating the cosine distance between centroid vectors of each pair of domains class-wisely as shown in Fig. 3. Note that the first row and first column of the $(N+1) \times (N+1)$ symmetric matrix for each class represent the distance of a specific domain to the source domain, while the diagonal elements denote the distance from each domain to itself, which are all zero.

Recall that for single-target domain adaptation, the strong representative set \mathcal{X}^{st} is formed by target samples close to the source domain, which can be easily extended to the multi-target domain case by selecting much closer samples from

peer domains based on the class-wise distance tensor \mathcal{G} . More specifically, let's consider a given target domain T_i . We are trying to identify another target domain, say T_j , which might be "more knowledgeable" about the source domain S than T_i . In that context, we apply the following two criteria to decide whether the j_{th} target domain is "more knowledgeable" about the source domain than the i_{th} target domain for a given class l :

- *Criterion 1:* $\mathcal{G}[0, j + 1, l] < \mathcal{G}[0, i + 1, l]$, which implies that the j_{th} target domain T_j is closer to the source domain than the i_{th} target domain T_i for class l .
- *Criterion 2:* $\mathcal{G}[i + 1, j + 1, l] < \mathcal{G}[0, i + 1, l]$, which implies that the j_{th} target domain T_j is in-between the source domain and the i_{th} target domain T_i for class l .

Fig. 4 gives a demonstration on how these two criteria work for three possible scenarios regarding the distance among target domain T_i , target domain T_j , and the source domain S . The distance to source domain from the first scenario-location of T_j is larger than T_i , which violates the first criterion. While for the second scenario location of T_j , it's on the other side of the source domain, therefore the second criterion is violated. The third scenario location satisfies both criteria, consequently T_j can be utilized as an in-between domain to help reduce the divergence between S and T_i .

Given the class-wise distance tensor \mathcal{G} , the updating strategy for strong representative set in the multi-target scenario can be found as follows. For a given class $l \in [1, k]$ in target domain T_i , we replace the original strong representative sample in \mathcal{X}_i^{st} with another one from the peer domains which satisfy the two criteria above. More specifically,

$$\mathcal{X}_i^{st}(l) = \begin{cases} \mathcal{X}_j^{st}(l) & \text{if criterion 1\& 2 satisfied} \\ \mathcal{X}_i^{st}(l), & \text{otherwise} \end{cases} \quad (7)$$

where $\mathcal{X}_i^{st}(l)$ represents the sample with label l in the strong representative set of the i_{th} target domain. Note that in the case where exists multiple representative samples from peer domains that satisfy the criteria, we randomly choose one from them to replace the corresponding sample in \mathcal{X}_i^{st} in order to improve the diversity of the representative samples. After that, a subset of training samples and their pseudo labels (X^{sw}, \hat{Y}^{sw}) are selected out in the same way as Eq. (6) to train the network. The framework for multi-target UDA is the same as that for single-target UDA as shown in Fig. 2 with the only difference on the updating strategy of the strong supervision set as introduced above.

2) *Pipeline for Multi-target UDA:* In practice, we find that training N baseline networks for all the N target domains in parallel makes the system complex. Therefore, we train each target domain separately using our single-target pipeline as shown in Fig. 2, and then select samples with prediction probability greater than a threshold λ from each class to form a pseudo strong representative set $\hat{\mathcal{X}}_i^{st}$ for each target domain T_i . Consequently, in the fusion and selection procedure, we slightly modify the multi-target fusion strategy in Eq. (7) by replacing the strong representative set \mathcal{X}_j^{st} with the pseudo strong representative set $\hat{\mathcal{X}}_j^{st}$. Then a baseline network is trained on the source domain and applied on the source domain

and all the N target domains to get the class-wise distance graph \mathcal{G} . After that, for each target domain in the multi-target UDA scenario, a single-target pipeline as shown in Fig. 2 is applied to train a baseline network with the target domain itself, the source domain, and the pseudo strong representative sets from peer domains.

The full pipeline of our strong-weak integrated semi-supervision multi-target domain adaptation is formed by three parts as shown in Alg. 2.

Algorithm 2 Strong-Weak Integrated Semi-Supervision for multi-target domain adaptation

Require: a labeled source domain S , N unlabeled target domains $\{T_i\}_{i=1}^N$

Ensure: N optimized baseline networks as Fig. 1

Part 1

for $i \in [1, N]$ **do**

pseudo $\hat{\mathcal{X}}_i^{st} \leftarrow$ train a single-target UDA network via Alg. 1

end for

Part 2

Train a baseline network with S only

$\mathcal{G} \leftarrow$ class-wise distance graph

Part 3

Given \mathcal{G} , $\{\hat{\mathcal{X}}_i^{st}\}_{i=1}^N$

for $i \in [1, N]$ **do**

for each iteration **do**

$L_{CE} \leftarrow$ forward a source batch (X^s, Y^s) to the i_{th} baseline network

Back-propagate L_{CE} , optimization

$L_{IM}, L_{ALL} \leftarrow$ forward a batch X^t to the i_{th} baseline network

$(X^{sw}, \hat{Y}^{sw}) \leftarrow$ sample replacing, fusion, selection

$L_{SW} \leftarrow$ forward (X^{sw}, \hat{Y}^{sw}) to the i_{th} baseline network

Back-propagate $k1L_{IM}+k2L_{ALL}+k3L_{SW}$, optimization

$\mathcal{X}_i^{wk} \leftarrow$ weak representative set updating

if reach certain iterations **then**

$\mathcal{X}_i^{st} \leftarrow$ strong representative set updating for T_i

end if

end for

end for

D. Loss Functions

1) *Source Domain Loss Functions:* For a labeled source batch, we utilize the standard Cross Entropy loss L_{CE} to train the network to minimize the classification error as follows:

$$L_{CE} = \frac{1}{b_s} \sum_{i=1}^{b_s} \sum_{j=1}^k -y_{ij} \log(p_{ij}) \quad (8)$$

where b_s is batch size, k is the number of classes, $y_{ij} = 1$ if the (ground truth) label of the i_{th} sample is j , otherwise $y_{ij} = 0$.

2) *Target Domain Loss Functions:* For the unlabeled target domain, we adopt the mutual information maximization loss L_{IM} [29], [36] as the baseline and propose a new adversarial logit loss as an improvement. The L_{IM} is based on the mutual information $I(X; \hat{Y})$ between the input X and the output \hat{Y} , namely, $I(X; \hat{Y}) = H(\hat{Y}) - H(\hat{Y}|X)$. L_{IM} is formulated as:

$$L_{IM} = \sum_{j=1}^k \hat{p}_j \log(\hat{p}_j) + \frac{1}{b_s} \sum_{i=1}^{b_s} \sum_{j=1}^k -p_{ij} \log(p_{ij}), \quad (9)$$

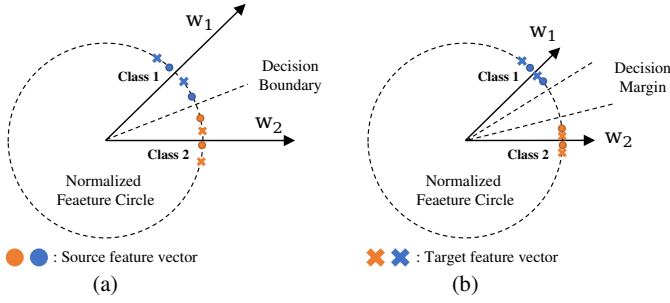


Fig. 5. A 2D illustration of the effect of the proposed adversarial logit loss L_{ALL} . (a) before L_{ALL} intra-class variance and domain divergence are large, (b) after L_{ALL} both intra-class variance and domain divergence are reduced. Note that due to the L_2 normalization, all the feature vectors are lying on the normalized feature circle with radius being τ (τ is the temperature).

where b_s is batch size, k is the number of classes, p_{ij} is the probability of a sample i belonging to class j , $\hat{p}_j = \frac{1}{b_s} \sum_{i=1}^{b_s} p_{ij}$ is the average probabilities of samples belonging to class j in a training batch with b_s samples. Note that the mutual information between X and \hat{Y} can also be reformulated as: $I(X; \hat{Y}) = H(X) - H(X|\hat{Y})$, which means that minimizing $H(X|\hat{Y})$ can also improve the performance. Given that $H(X|\hat{Y}) = \sum_{j=1}^k p_j H(X|\hat{Y} = j)$, we can see that the final goal is to minimize the conditional entropy of X given that it belongs to class j .

Recall that in our baseline network, the feature vector v fed into the classifier \mathbf{F} is normalized by a constant temperature τ . Therefore, the equation for the logit l_j between v and the j_{th} prototype can be reformulated as:

$$l_j = \mathbf{w}_j^T \cdot v = T \|\mathbf{w}_j^T\| \cos(\theta), \quad (10)$$

where \mathbf{w}_j is the j_{th} prototype, which is also the j_{th} weight vector in the classifier \mathbf{F} , θ is the angle between v and \mathbf{w}_j . We can see from the equation above that for a given class j , the prototype \mathbf{w}_j is constant for all the samples belonging to this class, therefore, a feasible way to reduce the intra-class variance of feature vectors is to minimize θ for those samples. In order to reduce the angle θ for target domain samples, we propose a novel adversarial logit loss which tries to enlarge $\cos(\theta)$ by reducing \mathbf{w}_j . More specifically, we formulate the adversarial logit loss L_{ALL} as:

$$L_{ALL} = \frac{1}{b_s} \sum_{i=1}^{b_s} \begin{cases} 0, & \text{otherwise} \end{cases} \quad (11)$$

where b_s is the batch size, l_{ij} is the logit value between sample i and class j , p_{ij} is the corresponding prediction probability. Eq. (11) implies that for a given input target domain sample, we firstly calculate its logits to each class in the forwarding path, then select the largest one as its contribution toward the overall value of the proposed adversarial loss L_{ALL} . Subsequently, L_{ALL} is back-propagated with a gradient reverse layer between the classifier \mathbf{F} and the rest of the network such that \mathbf{F} will try to minimize L_{ALL} by reducing the norm of prototypes, while the bottleneck layers and \mathbf{G} focus on maximizing L_{ALL} by decreasing the angle θ .

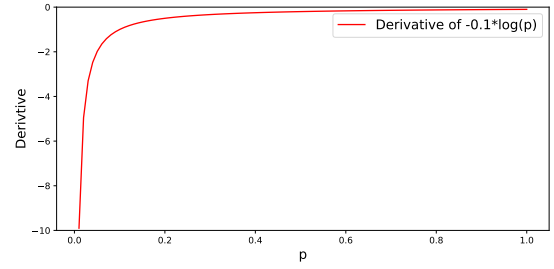


Fig. 6. Demonstration on the derivative of $-0.1 * \log(p)$. The derivative is close to 0 when p is large.

3) *Strong-weak Integrated Semi-supervision Loss Functions*: For the strong-weak integrated semi-supervision batch (X^{sw}, \hat{Y}^{sw}) , one straightforward approach is to use the Cross Entropy as the loss function. However, as shown in Fig. 6, we found that the derivative of the Cross Entropy is relatively small when the probability is approaching 1.0, which means that it's hard for the Cross Entropy loss to optimize the network when the pseudo-label is incorrectly estimated with a high confidence. Therefore, we design the following function for the strong-weak integrated semi-supervision loss L_{SW} :

$$L_{SW} = \frac{1}{b_s} \sum_{i=1}^{b_s} \sum_{j=1}^k y_{ij} (1.0 - p_{ij}) \quad (12)$$

which replaces $-\log(p_{ij})$ in Eq. (8) with $1.0 - p_{ij}$ such that the derivative is constant regardless of the probability.

As a summary, the overall optimization goal is:

$$\text{minimizing} \begin{cases} L_{CE} & \text{for } S \\ k_1 L_{IM} + k_2 L_{ALL} + k_3 L_{SW} & \text{for } T. \end{cases} \quad (13)$$

Details about the hyper-parameters k_1 , k_2 , k_3 will be discussed in the experimental section.

IV. EXPERIMENTS

A. Setup

We term our strong-weak integrated semi-supervision for single-target and multi-target domain adaptation as SWISS(single) and SWISS(multi), respectively. For quantitative assessment of the proposed method, we evaluate it on three popular benchmarks with more than two domains for unsupervised domain adaptation: Office-31 [37], Office-Home [38], DomainNet [5]; and, we compare our proposed method with state-of-the-art single-target and multi-target methods.

Office-31 [37] is a small-size benchmark that contains 31 classes of objects under the office environment. Three domains: Amazon (A) with 2817 samples, DSRL (D) with 498 samples, and Web (W) with 795 samples are included.

Office-Home [38] is a medium-size benchmark which contains 65 classes of objects under both office and home environments. Four domains: Art (Ar) with 2427 samples, Clipart (Cl) with 4365 samples, Product (Pr) with 4439 samples, and Real-World (Re) with 4357 samples are included. The Office-Home benchmark is much more challenging than the Office benchmark because samples in Art and Product domains usually contain complex background.

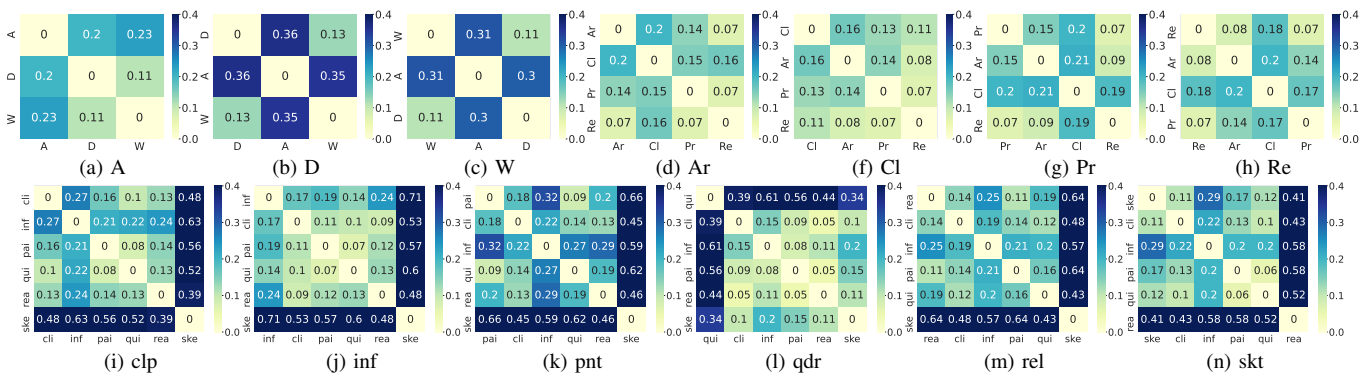


Fig. 7. The average of distance tensor \mathcal{G} over different classes for Office-31, Office-Home, and DomainNet. Lighter color means smaller distance.

DomainNet [5] is the largest benchmark so far which is formed by 0.6 million images from 345 classes. Six domains: Clipart (clp), Infograph (inf), Painting (pnt), Quickdraw (qdr), Real (rel) and Sketch (skt) are included, each of which contains a training set and a testing set. We train the domain adaptation network based on those training sets from each domain, and calculate accuracy on the testing sets.

Baselines. For single-target domain adaptation, we compare with several classical and state-of-the-art methods, namely, the classical DANN [39], MSTN [40], ADDA [41], MCD [42], RTN [43], JAN [44], CDAN+BSP [45], CAN [46], MDD [47], DCAN [48], SHOT-IM [29], MIMTFL [49], and the most recent FixBi [23], ATDOC [22], SCDA [50], AANet [7]. For multi-target domain adaptation, we compare with three recent works MT-MTDA [12], D-CGCT [14], and HGAN [9]. Notice that the quantitative results are cited from published papers because we follow the same setting as those papers on the Office, Office-Home, and DomainNet benchmarks.

Implementation Details We employ the pre-trained ResNet-50 or ResNet-101 as the feature generator \mathbf{G} like that in [20], [29], [48], [51], [52]. For the classifier \mathbf{F} , we use a linear layer with the input and output dimensions being $(1024, k)$, where k is the number of classes. The network is trained with the Stochastic Gradient Descent (SGD) optimizer with a momentum of 0.9. The learning rate is scheduled with the strategy in [19], which is formulated as $\eta_q = \frac{\eta_0}{(1+aq)^b}$ where q is the training progress linearly changed from 0 to 1, $a = 10$, $b = 0.75$, $\eta_0 = 0.01$ for \mathbf{F} and the bottleneck layers, and $\eta_0 = 0.001$ for \mathbf{G} . We use 48 as the training and testing batch size for all the experiments due to the limit of memory. The up-limit of training iterations for Office-31, Office-Home, and DomainNet are 3000, 5000, and 10000, respectively. The value of temperature τ in feature normalization is set to 20, following the results of [53], [54]. Similar to the setting in [29], we randomly run our method three times via PyTorch and report the average accuracy.

B. Results

Results on Office-31 The classification results for the small-size Office-31 dataset are presented in Table 1. Although our methods are not as accurate as the recent single-target works FixBi [23] and CAN [45], which significantly outperform other methods, both of our methods demonstrate similar

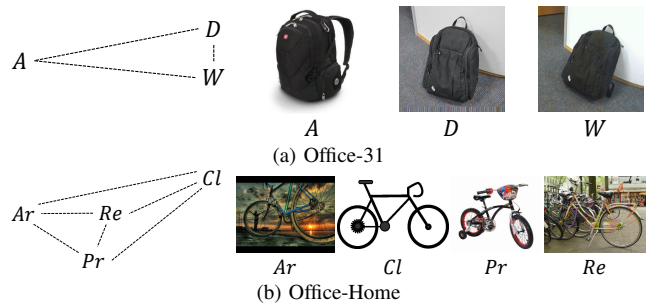


Fig. 8. The estimated topology relationship between domains and selected representative samples in Office-31 and Office-Home.

TABLE I
CLASSIFICATION ACCURACIES (%) ON SMALL-SIZE OFFICE-31 DATASET WITH BACKBONE RESNET-50.

Category	Method (S \rightarrow T)	A \rightarrow D	A \rightarrow W	D \rightarrow A	D \rightarrow W	W \rightarrow A	W \rightarrow D	Avg.
Single T.	SHOT-IM [29]	90.6	91.2	72.5	98.3	71.4	99.9	87.3
	DCAN [48]	90.7	92.7	73.5	98.4	73.4	100.	88.1
	CDAN+BSP [45]	93.0	93.3	73.6	98.2	72.6	100.	88.5
	AANet [7]	94.5	94.0	76.7	99.2	76.1	100.	90.1
	SCDA [50]	94.6	94.8	77.5	98.2	76.4	100.	90.3
	ATDOC [22]	95.4	94.6	77.5	98.1	77.0	99.7	90.4
	CAN [45]	95.0	94.5	78.0	99.1	77.0	99.8	90.6
FixBi [23]	95.0	96.1	78.7	99.3	79.4	100.	91.4	
Multi T.	MT-MTDA [12]		87.9		83.7		84.0	85.2
	HGAN [9]	87.8	88.2	71.4	97.5	69.9	100.0	85.8
	D-CGCT [14]		93.4		86.0		87.1	88.8
Our	SWISS(single)	94.8	93.6	76.5	98.6	77.1	99.8	90.1
	SWISS(multi)	94.7	94.3	77.1	98.6	77.0	99.8	90.3

performance to AANet [7], SCDA [50], and ATDOC [22] at the second level. However, when compared to the most recent multi-target methods MT-MTDA [12], HGAN [9], and D-CGCT [14], our SWISS(multi) exhibits a clear improvement of 1.5% over their best performance. Analyzing SWISS(multi) in comparison to SWISS(single), we observe improvements in sub-tasks A \rightarrow W and D \rightarrow A, while no improvement is observed for the sub-tasks D \rightarrow W and W \rightarrow D. The reason behind this phenomenon can be understood from Fig.7 (a)-(c), where it can be seen that the distance between A and D is slightly smaller than the distance between A and W in Fig.7 (a). This implies that D can aid in domain adaptation between A and W, and similarly, W can enhance performance when adapting from D to A, as depicted in Fig.7 (b). However, the distance from A to D or W is consistently larger than

TABLE II
CLASSIFICATION ACCURACIES (%) ON MEDIUM-SIZE OFFICE-HOME DATASET WITH BACKBONE RESNET-50.

Category	Method (S → T)	Ar → Cl	Ar → Pr	Ar → Re	Cl → Ar	Cl → Pr	Cl → Re	Pr → Ar	Pr → Cl	Pr → Re	Re → Ar	Re → Cl	Re → Pr	Avg.
Single T.	CDAN+BSP [45]	52.0	68.6	76.1	58.0	70.3	70.2	58.6	50.2	77.6	72.2	59.3	81.9	66.3
	SHOT-IM [29]	55.4	76.6	80.4	66.9	74.3	75.4	65.6	54.8	80.7	73.7	58.4	83.4	70.5
	DCAN [48]	57.9	76.2	79.3	67.3	76.1	75.6	65.4	56.0	80.7	74.2	61.2	84.2	71.2
	FixBi [23]	58.1	77.3	80.4	67.7	79.5	78.1	65.8	57.9	81.7	76.4	62.9	86.7	72.7
	AANet [7]	58.4	79.0	82.4	67.5	79.3	78.9	68.0	56.2	82.9	74.1	60.5	85.0	72.8
	SCDA [50]	60.7	76.4	82.8	69.8	77.5	78.4	68.9	59.0	82.7	74.9	61.8	84.5	73.1
	ATDOC [22]	60.2	77.8	82.2	68.5	78.6	77.9	68.4	58.4	83.1	74.8	61.5	87.2	73.2
Multi T.	MT-MTDA [12]		64.6			66.4			59.2			67.1		64.3
	D-CGCT [14]		70.5			71.6			66.0			71.2		69.8
Our	SWISS(single)	60.7	78.2	81.9	69.3	77.9	79.4	69.5	57.4	82.6	76.4	59.8	85.0	73.2
	SWISS(multi)	61.2	79.2	81.8	70.6	78.5	79.5	70.7	58.2	82.6	76.3	59.7	85.1	73.6

the distance between D and W, resulting in no improvement when adopting the domain between D and W. Furthermore, Fig.8(a) illustrates the estimated topology relationship between domains and representative samples in the Office-31 dataset, revealing that samples from D and W exhibit high similarity to each other but are distinct from those in A. Consequently, when D or W serves as the source domain, samples from A are unable to provide valuable information to mitigate domain divergence. It is important to note that Office-31 is a small dataset and the D and W domains contain only 498 and 795 samples respectively, which means that a 1.0% improvement corresponds to merely 5 to 8 accurately estimated samples. In the remainder of this section, we will demonstrate that our methods achieve significantly better performance than state-of-the-art methods in medium-size and large-size benchmarks.

Results on Office-Home In the more challenging medium-size Office-Home dataset, our SWISS(multi) achieves state-of-the-art performance, surpassing other methods by 0.4% at the second level (ATDOC [22] and SCDA [50]) and by 0.8% at the third level (AANet [7] and FixBi [23]), as shown in Table 2. Additionally, our SWISS(single) achieves an average accuracy of 73.1%, which is on par with ATDOC [22] and SCDA [50]. When comparing our methods to others, we observe that our approach outperforms competing methods, particularly in challenging tasks like Ar → Cl and Pr → Ar. Comparing SWISS(multi) to SWISS(single), we observe clear improvements in both the average accuracy and most sub-tasks, such as Ar → Cl, Ar → Pr, and Cl → Pr. The explanation for this can be found in Fig.8(b), which reveals that Ar, Pr, and Cl form a triangle with Re inside. This indicates that when any of the domains Ar, Pr, or Cl is the source domain, Re can serve as a useful peer domain to enhance the performance of sub-tasks. Conversely, when Re is the source domain, none of the domains Ar, Pr, or Cl can act as a useful peer domain to each other, resulting in no improvement of SWISS(multi) over SWISS(single) in the Re → Ar/Pr/Cl sub-tasks. The relationships between domains are further validated in Fig.7. For example, considering Ar as the source domain, we can observe from Fig.7(d) that the distance between Ar and Re ($dis_{Ar,Re} = 0.07$) is smaller than the distance between Ar and Cl ($dis_{Ar,Cl} = 0.2$), and the distance between Cl and Re ($dis_{Cl,Re} = 0.16$) is also smaller than $dis_{Ar,Cl}$. Thus, both criteria in Sec.III-C1 are satisfied, allowing domain Re to be utilized to aid the adaptation process of Ar → Cl. Comparing

our approach to the multi-target methods MT-MTDA [12] and D-CGCT [14], we observe a significant improvement of 3.8% with our SWISS(multi).

Results on DomainNet In the most challenging large-size DomainNet dataset, both our SWISS(single) and SWISS(multi) outperform state-of-the-art methods by a significant margin of approximately 2.0%. The details of sub-task accuracies are presented in Table 3, revealing that for the very challenging sub-tasks with accuracies below 20.0%, our SWISS(single) and SWISS(multi) exhibit a slight decrement of 1.0% and 0.6% on average compared to SCDA [50]. However, for sub-tasks with accuracies above 20.0%, our SWISS(single) and SWISS(multi) showcase a notable improvement of 3.1% and 3.3% on average, respectively, compared to SCDA [50]. One possible reason for this phenomenon is that the predicted labels of target samples are heavily influenced by errors in those very challenging sub-tasks. As a result, both strong supervision and weak supervision struggle to provide useful information for enhancing performance. However, for moderately challenging tasks, both of our methods exhibit significant improvements over SCDA [50] with a substantial margin. Tab. IV provides a comparison with additional methods for each source → rest direction. From the table, several observations can be made: 1) The state-of-the-art multi-target method D-CGCT [14] achieves a 1.1% improvement over the state-of-the-art single-target method SCDA [50]. 2) Our SWISS(single) and SWISS(multi) outperform D-CGCT [14] with a moderate margin of around 1.0%. Furthermore, our SWISS(multi) achieves the best scores in four out of six tasks among all the methods, demonstrating the effectiveness of our approach.

C. Model Analysis and Discussions

Parameter sensitivity. To analyze the impact of the hyper-parameters in our method, we evaluate the accuracies by varying each parameter while keeping others at their default settings. The four hyper-parameters are the weights k1, k2, k3 of the loss terms L_{IM} , L_{ALL} , L_{SW} and the threshold λ for the prediction probability in Eq. (4) and Eq. (11). We conduct experiments with different values for each parameter: k1={0.01, 0.05, 0.1, 0.2, 0.3, 0.4}, k2={0.01, 0.05, 0.1, 0.2, 0.3, 0.4}, k3={0.1, 0.5, 1.0, 2.0, 3.0, 4.0}, and λ ={0.9, 0.8, 0.7}. From Fig. 9(a)-(c), we observe that the combination of k1=0.1, k2=0.05, and k3=1.0 leads to the highest accuracy and

TABLE III

CLASSIFICATION ACCURACIES (%) ON LARGE-SIZE DOMAINNET DATASET WITH BACKBONE RESNET-101. THE CLASSIFICATION ACCURACY ARE REPORTED FOR EACH SOURCE→TARGET SUB-TASKS WITH SOURCE DOMAIN BEING INDICATED IN THE ROWS AND TARGET DOMAIN BEING INDICATED BY COLUMNS.

ADDA [41]	clp	inf	pnt	qdr	rel	skt	Avg.	DANN [39]	clp	inf	pnt	qdr	rel	skt	Avg.	MIMTFL [49]	clp	inf	pnt	qdr	rel	skt	Avg.
clp	-	11.2	24.1	3.2	41.9	30.7	22.2	clp	-	15.5	34.8	9.5	50.8	41.4	30.4	clp	-	15.1	35.6	10.7	51.5	43.1	31.2
inf	19.1	-	16.4	3.2	26.9	14.6	16.0	inf	31.8	-	30.2	3.8	44.8	25.7	27.3	inf	32.1	-	31.0	2.9	48.5	31.0	29.1
pnt	31.2	9.5	-	8.4	39.1	25.4	22.7	pnt	39.6	15.1	-	5.5	54.6	35.1	30.0	pnt	40.1	14.7	-	4.2	55.4	36.8	30.2
qdr	15.7	2.6	5.4	-	9.9	11.9	9.1	qdr	11.8	2.0	4.4	-	9.8	8.4	7.3	qdr	18.8	3.1	5.0	-	16.0	13.8	11.3
rel	39.5	14.5	29.1	12.1	-	25.7	24.2	rel	47.5	17.9	47.0	6.3	-	37.3	31.2	rel	48.5	19.0	47.6	5.8	-	39.4	32.1
skt	35.3	8.9	25.2	14.9	37.6	-	25.4	skt	47.9	13.9	34.5	10.4	46.8	-	30.7	skt	51.7	16.5	40.3	12.3	53.5	-	34.9
Avg.	28.2	9.3	20.1	8.4	31.1	21.7	19.8	Avg.	35.7	12.9	30.2	7.1	41.4	29.6	26.1	Avg.	38.2	13.7	31.9	7.2	45.0	32.8	28.1
ResNet-101 [1]	clp	inf	pnt	qdr	rel	skt	Avg.	CDAN [20]	clp	inf	pnt	qdr	rel	skt	Avg.	MDD [47]	clp	inf	pnt	qdr	rel	skt	Avg.
clp	-	19.3	37.5	11.1	52.2	41.0	32.2	clp	-	20.4	36.6	9.0	50.7	42.3	31.8	clp	-	20.5	40.7	6.2	52.5	42.1	32.4
inf	30.2	-	31.2	3.6	44.0	27.9	27.4	inf	27.5	-	25.7	1.8	34.7	20.1	22.0	inf	33.0	-	33.8	2.6	46.2	24.5	28.0
pnt	39.6	18.7	-	4.9	54.5	36.3	30.8	pnt	42.6	20.0	-	2.5	55.6	38.5	31.8	pnt	43.7	20.4	-	2.8	51.2	41.7	32.0
qdr	7.0	0.9	1.4	-	4.1	8.3	4.3	qdr	21.0	4.5	8.1	-	14.3	15.7	12.7	qdr	18.4	3.0	8.1	-	12.9	11.8	10.8
rel	48.4	22.2	49.4	6.4	-	38.8	33.0	rel	51.9	23.3	50.4	5.4	-	41.4	34.5	rel	52.8	21.6	47.8	4.2	-	41.2	33.5
skt	46.9	15.4	37.0	10.9	47.0	-	31.4	skt	50.8	20.3	43.0	2.9	50.8	-	33.6	skt	54.3	17.5	43.1	5.7	54.2	-	35.0
Avg.	34.4	15.3	31.3	7.4	40.4	30.5	26.6	Avg.	38.8	17.7	32.8	4.3	41.2	31.6	27.7	Avg.	40.4	16.6	34.7	4.3	43.4	32.3	28.6
SCDA [50]	clp	inf	pnt	qdr	rel	skt	Avg.	SWISS(single)	clp	inf	pnt	qdr	rel	skt	Avg.	SWISS(multi)	clp	inf	pnt	qdr	rel	skt	Avg.
clp	-	20.4	43.3	15.2	59.3	46.5	36.9	clp	-	19.6	46.8	15.9	62.8	49.3	38.9	clp	-	19.5	47.2	15.8	63.0	49.5	39.0
inf	32.7	-	34.5	6.3	47.6	29.2	30.1	inf	39.5	-	39.7	3.9	53.4	34.6	34.2	inf	40.4	-	40.2	4.0	53.6	34.2	34.5
pnt	46.4	19.9	-	8.1	58.8	42.9	35.2	pnt	50.0	19.2	-	5.4	60.1	45.0	36.0	pnt	50.0	19.6	-	6.9	60.1	45.4	36.4
qdr	31.1	6.6	18.0	-	28.8	22.0	21.3	qdr	34.9	5.9	18.2	-	30.4	24.7	22.8	qdr	35.5	6.8	19.5	-	30.5	24.7	23.4
rel	55.5	23.7	52.9	9.5	-	45.2	37.4	rel	58.3	21.8	54.3	6.9	-	46.9	37.6	rel	58.3	22.0	54.6	6.9	-	47.3	37.8
skt	55.8	20.1	46.5	15.0	56.7	-	38.8	skt	60.7	20.8	49.4	15.0	61.2	-	41.4	skt	60.8	20.7	49.6	14.8	61.5	-	41.5
Avg.	44.3	18.1	39.0	10.8	50.2	37.2	33.3	Avg.	48.7	17.5	41.7	9.4	53.6	40.1	35.2	Avg.	49.0	17.7	42.2	9.7	53.7	40.2	35.4

TABLE IV

CLASSIFICATION ACCURACIES (%) ON LARGE-SIZE DOMAINNET DATASET WITH BACKBONE RESNET-101. THE CLASSIFICATION ACCURACY ARE REPORTED FOR EACH SOURCE→REST DIRECTION, WITH EACH SOURCE DOMAIN BEING INDICATED IN THE COLUMNS.

Model	DomainNet						
	clp	inf	pnt	qdr	rel	skt	Avg.
Source train	25.6	16.8	25.8	9.2	20.6	22.3	20.1
SE [55]	21.3	8.5	14.5	13.8	16.0	19.7	15.6
MCD [42]	25.1	19.1	27.0	10.4	20.2	22.5	20.7
DADA [56]	26.1	20.0	26.5	12.9	20.7	22.8	21.5
CDAN [20]	31.6	27.1	31.8	12.5	33.2	35.8	28.7
MCC [57]	33.6	30.0	32.4	13.5	28.0	35.3	28.8
SCDA [50]	36.9	30.1	35.2	21.3	37.4	38.8	33.3
D-CGCT [14]	37.0	32.2	37.3	19.3	39.8	40.8	34.4
SWISS(multi)	39.0	34.5	36.4	23.4	37.8	41.5	35.4

exhibits relatively smaller sensitivity to parameter changes. Regarding the threshold λ , we find that setting $\lambda=0.8$ yields the best performance. Specifically, in both single-target and multi-target settings, $\lambda=0.9$ performs worse than $\lambda=0.8$, while $\lambda=0.7$ performs slightly better than $\lambda=0.8$ in the single-target setting but significantly worse in the multi-target setting. Therefore, we choose the values $k1=0.1$, $k2=0.05$, $k3=1.0$, and $\lambda=0.8$ for all our experiments.

TABLE V

CLASSIFICATION ACCURACIES (%) ON OFFICE-HOME WITH BACKBONE RESNET-50 UNDER DIFFERENT CONFIGURATIONS OF LOSS FUNCTIONS. THE AVERAGE ACCURACIES ARE REPORTED FOR EACH SOURCE IN THE COLUMNS WHICH ARE EVALUATED ON THE SINGLE-TARGET SETTING.

Method	Ar	Cl	Pr	Re	Avg.
ResNet50 [1]	47.6	41.8	43.4	51.7	46.1
+ L_{IM}	71.5	73.4	66.9	71.5	70.8
+ $L_{IM} + L_{ALL}$	73.2	73.7	68.5	72.5	72.0
+ $L_{IM} + L_{SW}$	72.3	74.4	67.7	73.2	71.9
+ $L_{ALL} + L_{SW}$	72.6	73.7	68.6	73.5	72.1
+ $L_{IM} + L_{ALL} + L_{SW}$	73.6	75.5	69.8	73.7	73.2

TABLE VI

CLASSIFICATION ACCURACIES (%) ON OFFICE-HOME WITH BACKBONE RESNET-50 UNDER DIFFERENT CONFIGURATIONS OF NETWORK COMPONENT.

Category	Method	Ar→ Cl	Ar→ Pr	Ar→ Re	Avg.
Single T.	Baseline Network + Strong	60.7	77.7	81.5	73.3
	Baseline Network + Weak	60.2	78.3	81.7	73.4
	Baseline Network + Strong + Weak	60.7	78.2	81.9	73.6
Multi T.	Baseline Network + Strong	60.7	77.7	81.3	73.2
	Baseline Network + Weak	60.4	78.3	82.0	73.6
	Baseline Network + Strong + Weak	61.2	79.2	81.8	74.1

Ablation study on different losses. Tab. V shows the classification accuracies on the Office-Home dataset with different configurations of loss functions. Comparing the results to the baseline ResNet50 [1], we can observe the effectiveness of the mutual information maximization loss L_{IM} , which is adopted from previous works [29], [36]. Furthermore, we can see clear improvements when incorporating the proposed adversarial logit loss L_{ALL} and the strong-weak integrated semi-supervision loss L_{SW} . By comparing the configurations + $L_{IM} + L_{ALL}$ and + $L_{IM} + L_{SW}$ with + L_{IM} , we achieve improvements of 1.2% and 1.1% for L_{ALL} and L_{SW} , respectively. Moreover, the configuration + $L_{ALL} + L_{SW}$ achieves similar performance to + $L_{IM} + L_{ALL}$ and + $L_{IM} + L_{SW}$, which highlights the effectiveness of the proposed loss functions. By combining all three loss functions, we achieve the best performance among all the configurations, with an average improvement of 2.2% over L_{IM} . This significant improvement demonstrates the advantages of our proposed method.

Ablation study on network components. To evaluate the effectiveness of the proposed strong-weak integrated semi-supervision strategy, we conducted experiments on the Office-Home dataset with Ar as the source domain. Tab. VI shows the accuracies of different configurations of network components,

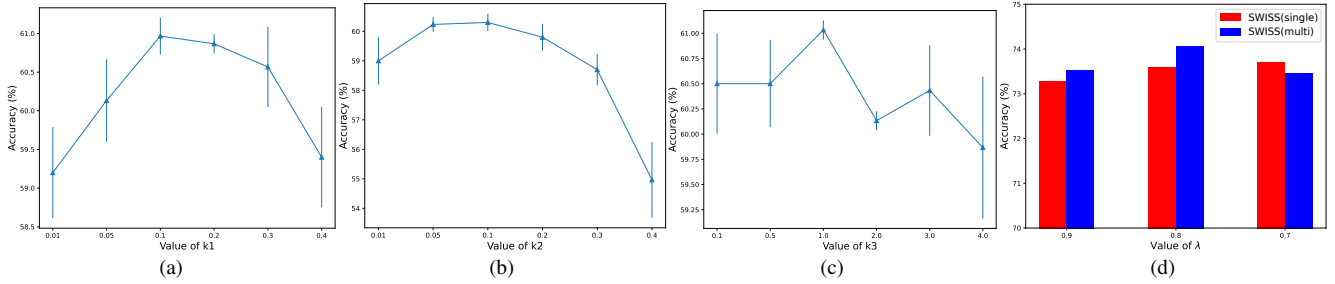


Fig. 9. Parameter sensitivity analysis with (a) $k1=\{0.01, 0.05, 0.1, 0.2, 0.3, 0.4\}$, (b) $k2=\{0.01, 0.05, 0.1, 0.2, 0.3, 0.4\}$, (c) $k3=\{0.1, 0.5, 1.0, 2.0, 3.0, 4.0\}$, and (d) $\lambda=\{0.9, 0.8, 0.7\}$. For (a)-(c), we evaluate in task $Ar \rightarrow Cl$. For (d), we show the average accuracies of $Ar \rightarrow \{Cl, Pr, Re\}$ in both single-target and multi-target settings.

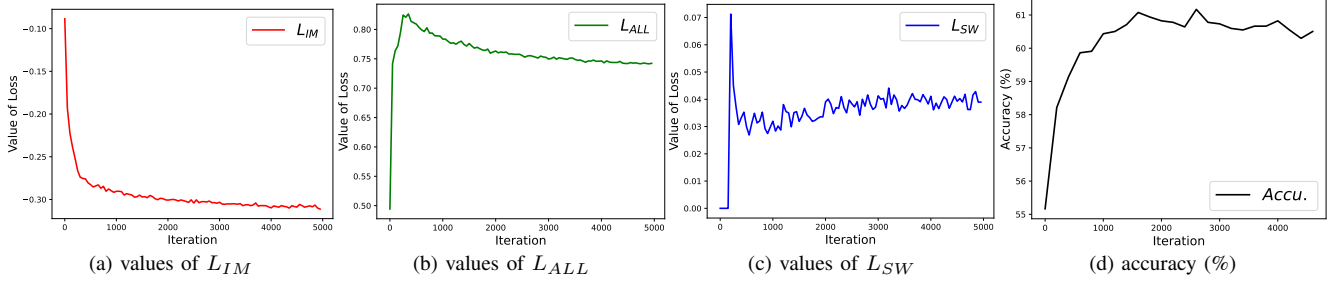


Fig. 10. Values of three loss terms L_{IM} , L_{ALL} , L_{SW} and the accuracy during training procedure for the sub-task $Ar \rightarrow Cl$ in Office-Home dataset.

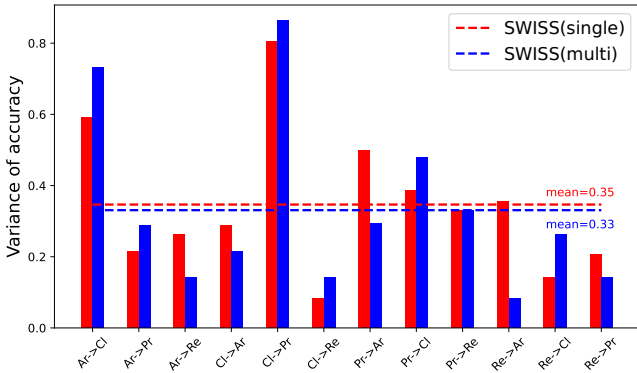


Fig. 11. Variances of accuracy for each sub-task in Office-Home for both single-target and multi-target setting.

namely, strong supervision only, weak supervision only, and strong-weak integrated semi-supervision. Comparing “Baseline Network + Strong” with “Baseline Network + Weak”, we observe that strong supervision tends to outperform weak supervision in the challenging task $Ar \rightarrow Cl$ but underperforms in the easier tasks $Ar \rightarrow Pr$ and $Ar \rightarrow Re$. This can be rationalized by the fact that strong supervision is more reliable than weak supervision when the prediction error is relatively high in challenging cases. However, in the easy cases, weak supervision provides similar prediction accuracy but offers greater sample variety. As a result, weak supervision can provide more informative signals, leading to better performance. The combination of strong supervision and weak supervision achieves the best performance in both the single-target and multi-target settings, with a margin of 0.35% in average. This result demonstrates the effectiveness of the proposed strong-weak integrated semi-supervision strategy.

Training stability. We investigated the accuracy and the

values of three loss terms, namely L_{IM} , L_{ALL} , and L_{SW} , during the training process for the $Ar \rightarrow Cl$ task. Fig. 10 illustrates the trends of these loss terms over iterations. Regarding L_{IM} , we observed a rapid decrease in its value, which converged after approximately 1000 iterations. This behavior is consistent with the findings in the work of [29]. For the proposed adversarial logit loss L_{ALL} , we observed that it initially experienced a significant jump in value within the first 500 iterations. This jump is caused by the optimization of the source domain loss term in Eq. (8), which increases the logit values to generate high probabilities for the source domain samples. Subsequently, the proposed adversarial logit loss continuously reduces the logit values, resulting in a gradual decrease and convergence of the loss after approximately 3000 iterations. As for L_{SW} shown in Fig. 10(c), its value remained at 0 for the first 200 iterations, indicating that it was not activated initially as mentioned in Sec. III-B3. Afterward, we observed a rapid drop in the value of L_{SW} from a large initial value, followed by convergence to a very small value. Regarding the testing accuracy shown in Fig. 10(d), we observed a quick increase in accuracy during the initial training iterations, which then converged to a value between 60.0% and 61.0%. Additionally, Fig. 11 displays the variances of the testing accuracy. We observed that, except for the $Ar \rightarrow Cl$ and $Cl \rightarrow Pr$ sub-tasks, the variances were generally smaller than the average values. Specifically, the average variances were 0.35 and 0.33 for the single-target and multi-target settings, respectively.

Visualization. To visualize the distributions of feature representations after domain adaptation, we employed the t-SNE method [58]. Fig.12 illustrates the values of the angle θ and L_2 norm in Eq. (10), as well as the feature distribution in the source and target domains under different configurations of loss terms. From the first row of Fig.12, we observed that

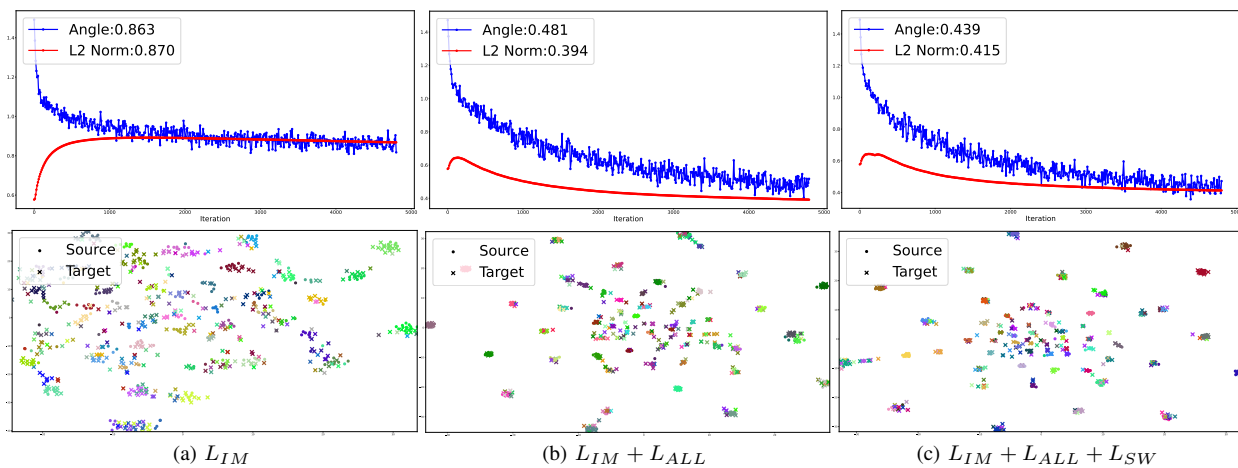


Fig. 12. Values of feature-prototype angle θ and L_2 norm of the prototype in Eq. (10), and the distribution of feature vectors in source and target domain under different configurations of loss terms for the sub-task Ar \rightarrow Cl in Office-Home dataset. For the distributions in the second rows, only 10% samples in the source and target domains are utilized for better view, we also use different colors to denote different classes.

the proposed adversarial loss L_{ALL} effectively reduced the L_2 norm of the prototype and the feature-prototype angle, as indicated by the decreasing values of θ and the L_2 norm. This reduction suggests a smaller intra-class domain divergence. Moreover, by comparing the third column with the second column, we observed that the addition of L_{SW} further reduced the angle. These findings are consistent with the results obtained from the t-SNE figures shown in the second row of Fig.12. Analyzing the t-SNE figures, we observed that the feature distribution obtained using only L_{IM} appeared relatively sparse. However, incorporating L_{ALL} made the distribution more compact within each class and more distinct/separated among different classes. Furthermore, the addition of L_{SW} led to further concentration of the feature distribution. Overall, these results demonstrate the effectiveness of the proposed loss terms in reducing intra-class domain divergence and enhancing the compactness and separability of the feature representations.

V. CONCLUSION

This paper presents a unified framework which adopts a novel strong-weak integrated semi-supervision strategy for both single target and multi target domain adaptation. A strong representative set with high prediction confidence but low diversity and a weak representative set with low prediction confidence but high diversity are maintained and updated during the training process. The fusion of them generates augmented training samples with pseudo-label, which are utilized as supervision for training the network. The extension from single to multi target domain adaptation is achieved by adopting the peer scaffolding strategy, which updates the strong representative set with samples not only from the target domain itself but also from its peer domains. Moreover, a novel adversarially optimized loss based on the logit instead of the probability is developed to further reduce the intra-class domain divergence. Comprehensive experiments on several popular benchmarks have demonstrated the effectiveness of the proposed method. In the future, the extension from our work to multi source domain adaptation can also be investigated.

REFERENCES

- [1] K. He, X. Zhang, S. Ren, and J. Sun, "Deep residual learning for image recognition," in *Proceedings of the IEEE Conference on Computer Vision and Pattern Recognition*, 2016, pp. 770–778.
- [2] S. Ren, K. He, R. Girshick, and J. Sun, "Faster r-cnn: Towards real-time object detection with region proposal networks," *IEEE Transactions on Pattern Analysis and Machine Intelligence*, vol. 39, no. 6, pp. 1137–1149, 2016.
- [3] M. Hniewa and H. Radha, "Integrated multiscale domain adaptive yolo," *IEEE Transactions on Image Processing*, vol. 32, pp. 1857–1867, 2023.
- [4] V. Badrinarayanan, A. Kendall, and R. Cipolla, "Segnet: A deep convolutional encoder-decoder architecture for image segmentation," *IEEE Transactions on Pattern Analysis and Machine Intelligence*, vol. 39, no. 12, pp. 2481–2495, 2017.
- [5] X. Peng, Q. Bai, X. Xia, Z. Huang, K. Saenko, and B. Wang, "Moment matching for multi-source domain adaptation," in *Proceedings of the IEEE International Conference on Computer Vision*, 2019, pp. 1406–1415.
- [6] A. Gretton, K. Borgwardt, M. Rasch, B. Schölkopf, and A. J. Smola, "A kernel method for the two-sample-problem," in *Advances in Neural Information Processing Systems*, 2007, pp. 513–520.
- [7] H. Xia, H. Zhao, and Z. Ding, "Adaptive adversarial network for source-free domain adaptation," in *Proceedings of the IEEE/CVF International Conference on Computer Vision*, 2021, pp. 9010–9019.
- [8] I. Goodfellow, J. Pouget-Abadie, M. Mirza, B. Xu, D. Warde-Farley, S. Ozair, A. Courville, and Y. Bengio, "Generative adversarial nets," in *Advances in Neural Information Processing Systems*, 2014, pp. 2672–2680.
- [9] X. Yang, C. Deng, T. Liu, and D. Tao, "Heterogeneous graph attention network for unsupervised multiple-target domain adaptation," *IEEE Transactions on Pattern Analysis and Machine Intelligence*, 2020.
- [10] Y. Wang, Z. Zhang, W. Hao, and C. Song, "Attention guided multiple source and target domain adaptation," *IEEE Transactions on Image Processing*, vol. 30, pp. 892–906, 2020.
- [11] B. Gholami, P. Sahu, O. Rudovic, K. Bousmalis, and V. Pavlovic, "Unsupervised multi-target domain adaptation: An information theoretic approach," *IEEE Transactions on Image Processing*, vol. 29, pp. 3993–4002, 2020.
- [12] L. T. Nguyen-Meidine, A. Belal, M. Kiran, J. Dolz, L.-A. Blais-Morin, and E. Granger, "Unsupervised multi-target domain adaptation through knowledge distillation," in *Proceedings of the IEEE/CVF Winter Conference on Applications of Computer Vision*, 2021, pp. 1339–1347.
- [13] T. Isobe, X. Jia, S. Chen, J. He, Y. Shi, J. Liu, H. Lu, and S. Wang, "Multi-target domain adaptation with collaborative consistency learning," in *Proceedings of the IEEE/CVF Conference on Computer Vision and Pattern Recognition*, 2021, pp. 8187–8196.
- [14] S. Roy, E. Krivosheev, Z. Zhong, N. Sebe, and E. Ricci, "Curriculum graph co-teaching for multi-target domain adaptation," in *Proceedings of the IEEE/CVF Conference on Computer Vision and Pattern Recognition*, 2021, pp. 5351–5360.

- [15] L. S. Vygotsky, *Mind in society: The development of higher psychological processes*. Harvard university press, 1980.
- [16] X. Lu and H. Radha, "Strong-weak integrated semi-supervision for unsupervised domain adaptation," in *2022 IEEE International Conference on Image Processing (ICIP)*. IEEE, 2022, pp. 2226–2230.
- [17] E. Tzeng, J. Hoffman, N. Zhang, K. Saenko, and T. Darrell, "Deep domain confusion: Maximizing for domain invariance," *arXiv preprint arXiv:1412.3474*, 2014.
- [18] M. Long, Y. Cao, J. Wang, and M. Jordan, "Learning transferable features with deep adaptation networks," in *International Conference on Machine Learning*. PMLR, 2015, pp. 97–105.
- [19] Y. Ganin, E. Ustinova, H. Ajakan, P. Germain, H. Larochelle, F. Laviolette, M. Marchand, and V. Lempitsky, "Domain-adversarial training of neural networks," *The Journal of Machine Learning Research*, vol. 17, no. 1, pp. 2096–2030, 2016.
- [20] M. Long, Z. Cao, J. Wang, and M. I. Jordan, "Conditional adversarial domain adaptation," in *Advances in Neural Information Processing Systems*, 2018, pp. 1640–1650.
- [21] Z. Du, J. Li, H. Su, L. Zhu, and K. Lu, "Cross-domain gradient discrepancy minimization for unsupervised domain adaptation," in *Proceedings of the IEEE/CVF Conference on Computer Vision and Pattern Recognition*, 2021, pp. 3937–3946.
- [22] J. Liang, D. Hu, and J. Feng, "Domain adaptation with auxiliary target domain-oriented classifier," in *Proceedings of the IEEE/CVF Conference on Computer Vision and Pattern Recognition*, 2021, pp. 16 632–16 642.
- [23] J. Na, H. Jung, H. J. Chang, and W. Hwang, "Fixbi: Bridging domain spaces for unsupervised domain adaptation," in *Proceedings of the IEEE/CVF Conference on Computer Vision and Pattern Recognition*, 2021, pp. 1094–1103.
- [24] Z. Hu, Z. Yang, X. Hu, and R. Nevatia, "Simple: Similar pseudo label exploitation for semi-supervised classification," in *Proceedings of the IEEE/CVF Conference on Computer Vision and Pattern Recognition*, 2021, pp. 15 099–15 108.
- [25] Z. Cai, A. Ravichandran, S. Maji, C. Fowlkes, Z. Tu, and S. Soatto, "Exponential moving average normalization for self-supervised and semi-supervised learning," in *Proceedings of the IEEE/CVF Conference on Computer Vision and Pattern Recognition*, 2021, pp. 194–203.
- [26] A. Abuduweili, X. Li, H. Shi, C.-Z. Xu, and D. Dou, "Adaptive consistency regularization for semi-supervised transfer learning," in *Proceedings of the IEEE/CVF Conference on Computer Vision and Pattern Recognition*, 2021, pp. 6923–6932.
- [27] W. Hu, T. Miyato, S. Tokui, E. Matsumoto, and M. Sugiyama, "Learning discrete representations via information maximizing self-augmented training," *arXiv preprint arXiv:1702.08720*, 2017.
- [28] J. Choi, M. Jeong, T. Kim, and C. Kim, "Pseudo-labeling curriculum for unsupervised domain adaptation," in *British Machine Vision Conference (BMVC)*. Springer, 2019.
- [29] J. Liang, D. Hu, and J. Feng, "Do we really need to access the source data? source hypothesis transfer for unsupervised domain adaptation," *arXiv preprint arXiv:2002.08546*, 2020.
- [30] M. Riazi, M. Rezaei *et al.*, "Teacher-and peer-scaffolding behaviors: Effects on efl students' writing improvement," in *Clesol 2010: Proceedings of the 12th national conference for community languages and ESOL*, 2011, pp. 55–63.
- [31] M. Pifarre and R. Cobos, "Promoting metacognitive skills through peer scaffolding in a cscl environment," *International Journal of Computer-Supported Collaborative Learning*, vol. 5, no. 2, pp. 237–253, 2010.
- [32] H. Daume III and D. Marcu, "Domain adaptation for statistical classifiers," *Journal of Artificial Intelligence Research*, vol. 26, pp. 101–126, 2006.
- [33] B. Sun and K. Saenko, "Deep coral: Correlation alignment for deep domain adaptation," in *European Conference on Computer Cision*. Springer, 2016, pp. 443–450.
- [34] S. Ben-David, J. Blitzer, K. Crammer, A. Kulesza, F. Pereira, and J. W. Vaughan, "A theory of learning from different domains," *Machine learning*, vol. 79, no. 1-2, pp. 151–175, 2010.
- [35] A. Gretton, K. M. Borgwardt, M. J. Rasch, B. Schölkopf, and A. Smola, "A kernel two-sample test," *The Journal of Machine Learning Research*, vol. 13, no. 1, pp. 723–773, 2012.
- [36] S. Li, M. Xie, K. Gong, C. H. Liu, Y. Wang, and W. Li, "Transferable semantic augmentation for domain adaptation," in *Proceedings of the IEEE/CVF Conference on Computer Vision and Pattern Recognition*, 2021, pp. 11 516–11 525.
- [37] K. Saenko, B. Kulis, M. Fritz, and T. Darrell, "Adapting visual category models to new domains," in *European Conference on Computer Vision*. Springer, 2010, pp. 213–226.
- [38] H. Venkateswara, J. Eusebio, S. Chakraborty, and S. Panchanathan, "Deep hashing network for unsupervised domain adaptation," in *Proceedings of the IEEE Conference on Computer Vision and Pattern Recognition*, 2017, pp. 5018–5027.
- [39] Y. Ganin and V. Lempitsky, "Unsupervised domain adaptation by backpropagation," in *International Conference on Machine Learning*. PMLR, 2015, pp. 1180–1189.
- [40] S. Xie, Z. Zheng, L. Chen, and C. Chen, "Learning semantic representations for unsupervised domain adaptation," in *International conference on machine learning*. PMLR, 2018, pp. 5423–5432.
- [41] E. Tzeng, J. Hoffman, K. Saenko, and T. Darrell, "Adversarial discriminative domain adaptation," in *Proceedings of the IEEE Conference on Computer Vision and Pattern Recognition*, 2017, pp. 7167–7176.
- [42] K. Saito, K. Watanabe, Y. Ushiku, and T. Harada, "Maximum classifier discrepancy for unsupervised domain adaptation," in *Proceedings of the IEEE Conference on Computer Vision and Pattern Recognition*, 2018, pp. 3723–3732.
- [43] M. Long, H. Zhu, J. Wang, and M. I. Jordan, "Unsupervised domain adaptation with residual transfer networks," *arXiv preprint arXiv:1602.04433*, 2016.
- [44] —, "Deep transfer learning with joint adaptation networks," in *International Conference on Machine Learning*. PMLR, 2017, pp. 2208–2217.
- [45] X. Chen, S. Wang, M. Long, and J. Wang, "Transferability vs. discriminability: Batch spectral penalization for adversarial domain adaptation," in *International Conference on Machine Learning*, 2019, pp. 1081–1090.
- [46] G. Kang, L. Jiang, Y. Yang, and A. G. Hauptmann, "Contrastive adaptation network for unsupervised domain adaptation," in *Proceedings of the IEEE Conference on Computer Vision and Pattern Recognition*, 2019, pp. 4893–4902.
- [47] Y. Zhang, T. Liu, M. Long, and M. Jordan, "Bridging theory and algorithm for domain adaptation," in *International Conference on Machine Learning*. PMLR, 2019, pp. 7404–7413.
- [48] P. Ge, C.-X. Ren, D.-Q. Dai, and H. Yan, "Domain adaptation and image classification via deep conditional adaptation network," *arXiv preprint arXiv:2006.07776*, 2020.
- [49] J. Gao, Y. Hua, G. Hu, C. Wang, and N. M. Robertson, "Reducing distributional uncertainty by mutual information maximisation and transferable feature learning," in *European Conference on Computer Vision*. Springer, 2020, pp. 587–605.
- [50] S. Li, M. Xie, F. Lv, C. H. Liu, J. Liang, C. Qin, and W. Li, "Semantic concentration for domain adaptation," in *Proceedings of the IEEE/CVF International Conference on Computer Vision*, 2021, pp. 9102–9111.
- [51] M. Chen, S. Zhao, H. Liu, and D. Cai, "Adversarial-learned loss for domain adaptation," *arXiv*, vol. abs/2001.01046, 2020.
- [52] R. Xu, G. Li, J. Yang, and L. Lin, "Larger norm more transferable: An adaptive feature norm approach for unsupervised domain adaptation," in *Proceedings of the IEEE International Conference on Computer Vision*, 2019, pp. 1426–1435.
- [53] K. Saito, D. Kim, S. Sclaroff, T. Darrell, and K. Saenko, "Semi-supervised domain adaptation via minimax entropy," in *Proceedings of the IEEE International Conference on Computer Vision*, 2019, pp. 8050–8058.
- [54] R. Ranjan, C. D. Castillo, and R. Chellappa, "L2-constrained softmax loss for discriminative face verification," *arXiv preprint arXiv:1703.09507*, 2017.
- [55] G. French, M. Mackiewicz, and M. Fisher, "Self-ensembling for visual domain adaptation," *arXiv preprint arXiv:1706.05208*, 2017.
- [56] X. Peng, Z. Huang, X. Sun, and K. Saenko, "Domain agnostic learning with disentangled representations," in *International Conference on Machine Learning*. PMLR, 2019, pp. 5102–5112.
- [57] Y. Jin, X. Wang, M. Long, and J. Wang, "Minimum class confusion for versatile domain adaptation," in *European Conference on Computer Vision*. Springer, 2020, pp. 464–480.
- [58] L. v. d. Maaten and G. Hinton, "Visualizing data using t-sne," *Journal of machine learning research*, vol. 9, no. Nov, pp. 2579–2605, 2008.